Finite-temperature calculations of the Compton profile of Be, Li, and Si

E. Klevak, F. D. Vila, J. J. Kas, J. J. Rehr, and G. T. Seidler

Phys. Rev. B **94**, 214201 — Published 2 December 2016

DOI: 10.1103/PhysRevB.94.214201

Finite temperature calculations of the Compton profile of Be, Li and Si.

E. Klevak, F. D. Vila, J. J. Kas, J. J. Rehr and G. T. Seidler
Department of Physics, University of Washington, Seattle, WA 98195
(Dated: October 26, 2016)

High resolution inelastic x-ray scattering experiments are widely used to study the electronic and chemical properties of materials under a range of conditions, from ambient temperature to the warm dense matter regime (WDM). We use the real-space multiple scattering (RSMS) Green's function formalism coupled with density functional theory molecular dynamics (DFT-MD) to study thermal effects on the CP of disordered systems. The RSMS method is advantageous for calculations of highly disordered, aperiodic systems because it places no restriction on symmetry. As a test, we apply our approach to thermally disordered Be, Li, and Si in both liquid and solid phases. We find good agreement with experimental and other theoretical results, showing that the real-space multiple scattering approach coupled with DFT-MD is an efficient and reliable method for calculating the CP of disordered systems at finite temperatures.

PACS numbers:
Keywords: WDM, XRTS, Be, Li, Si, Compton Profile, Thermal disorder

I. INTRODUCTION

The high resolution Compton profile (CP) is widely used to investigate the electronic and chemical properties of materials.[1–6] For metallic systems, it can be used to probe the Fermi surface and its behavior as a function of temperature and density. In materials that undergo phase transitions, the CP has proven to be a useful technique to distinguish and characterize different phases. For instance, in the solid to liquid phase transition in Si, CP analysis revealed persistent covalent bonding in the liquid phase.[6,7] CP at momentum values larger than the reciprocal lattice vector **G** (high momentum components) are sensitive to anharmonic and thermal disorder effects, and can be used in the study of thermal effects on the valence electrons.[6,8,9]

A variety of methods have been used to compute CPs. For example, *ab initio* band structure methods have been widely used for periodic systems. Their application to studies of electronic properties in disordered systems though, is more challenging. Early theoretical calculations of CPs in thermally disordered materials used the self-consistent temperature-dependent Linear Muffin-Tin Orbital (LMTO) method[10–12] based on local density approximation (LDA) with a frozen supercell of eight atoms, where the disorder was generated using Boltzmann statistical averages over atomic configurations generated from Gaussian distributions along the harmonic phonon modes.[13] This early approach was used to study thermal disorder effects in Li and predicted a broadening of the CP due to the thermal disorder. However, that investigation neglected thermal lattice expansion, which was later found to be a dominant effect in Al, Li and Be, negating the thermal broadening due to vibrational disorder.[8,9,14,15] Although this later study gave a good explanation of thermal effects, the theory employed empirical parameters to incorporate thermal effects, and therefore, its predictive capability is limited.

Another widely used theoretical method for calculating CPs is the Korringa-Kohn-Rostoker (KKR) and Coherent Potential Approximation (CPA) approach,[16] which has been applied to systems such as substitutionally disordered alloys. KKR uses a coherent potential approximation, where the disordered alloy is replaced with an ordered system with an averaged effective site potential.[17] Correlation corrections have also been applied[18] and used in the study of Li.[19] Differences between theory and experiment in the Li study were attributed to the effects of correlation on the momentum density beyond the LDA. Further investigations of electronic correlation beyond the quasiparticle approximation reported that the excitation of plasmarons produce a broadening of the CP.[20]

The GW approximation has also been used as a method for treating correlation effects beyond density functional theory. Early results in Li showed CPs that are very close to experiment.[21] However a later critique found that numerical instability played a role in those results.[22] Later studies[23,24] of the electron momentum density (EMD) of Li are based on modified augmented plane wave method with full potential and Lam-Platzman correlation corrections,[18] give a moderately good description of spectra. However, plane wave based methods are not ideally suited for calculations of highly disordered systems, because they require very large supercells. A later study accounted for thermal effects beyond the harmonic approximation,[25] as well as zero-point motion, using the *ab initio* beyond harmonic approximation,[26] and found excellent agreement with the experimental results. However, one can expect that at temperatures well above the Debye Einstein-temperature that zero-point motion will play a minor role.

More recent studies have used MD simulations to generate structural configurations for thermally disordered materials, in an attempt to obtain better electronic structure properties. In the case of ice,[27,28] anisotropy in the CP was studied using maximally localized Wannier functions coupled with Car-Parrinello molecular dynamics[29] (CPMD) simulations. The CPMD approach was used

to investigate the solid-liquid phase transition in Si and B,[6,7] where differences in the CPs of the two phases were attributed mainly to covalent bond breaking, while thermal disorder produced relatively small effects.[6]

In this paper we report *ab initio* calculations of the CP in the impulse approximation (IA), as well as calculations of the EMD, using a real-space Green's function (RSGF) approach coupled with DFT-MD simulations in order to include thermal disorder effects.

Unlike band structure calculations, RSGF approach coupled with MD simulations has the advantage of not being limited to crystalline systems. It also allows efficient calculations of valence electron properties of materials as a function of thermal disorder and thermal expansion, making it well suited to investigate liquids and solids over a wide range of temperatures from zero temperature to the WDM regime. The RSGF approach is implemented in FEFF9[43] code, which is widely used in the x-ray spectroscopy community. It has capabilities of calculating non-resonant inelastic x-ray scattering (NIXS) core contributions[30] and valence CP in the IA.[31] Here we apply this approach to thermally disordered Be, Li and Si, and compare our results to experimental[6,8,9] and other theoretical results, including recent results based on CPMD calculations.[6,7] We focus particularly on the high momentum components of the CP. We find that in Li, directional anisotropy of the CP decreases as a function of temperature, consistent with the observations of Erba et al. Refs. 25 in the case of LiF.

This paper is organized as follows: in section II, we give a brief overview of key equations. In section III, we present details of molecular dynamic (MD) simulations and CP calculations using FEFF. In section IV, we present results of the CP calculations for Be, Li and Si. We discuss in detail anharmonic and thermal disorder effects on the CP and the influence on high momentum components of CP. Finally, in section V, we present and discuss our conclusions.

II. COMPTON SCATTERING THEORY

Non-resonant inelastic x-ray scattering (NIXS) in the limit of large momentum transfer, often called Compton scattering, is directly related to the CP. Experimentally, the system is probed by a narrow x-ray beam incident on the sample and the intensity of scattered radiation is measured as a function of energy and scattering angle. In this two-photon process, the double differential scattering cross section (DDSC) $d^2\sigma\,(\mathbf{q},\,\omega)/d\Omega d\omega_2$ is measured, where Ω is the measured solid angle and ω_2 is the detected energy of radiation, and $\mathbf{q}$ and ω are, respectively, the momentum and energy transferred to the sample. Thus, the DDSC determines the relative probability of transferring momentum $\mathbf{q}$ and energy ω to the sample in the scattering process. Here we focus on cases where the incident energy in the XRTS experiment is far larger than any binding energy in the sample. In this regime, first order perturbation theory shows that the main contribution arises from the dominant $\mathbf{A}^2$ term in the interaction Hamiltonian, where $\mathbf{A}$ is the vector potential.[32] In the non-relativistic limit, the DDSC is given by

$$\frac{d^2\sigma}{d\,\Omega\,d\,\omega_2} = \left(\frac{d\,\sigma}{d\,\Omega}\right)_{\rm Th} S(\mathbf{q},\,\omega). \tag{1}$$

Here, the Thompson scattering cross section is

$$\left(\frac{d\,\sigma}{d\,\Omega}\right)_{\rm Th} = \frac{\omega_2}{\omega_1} r_0^2 (\hat{\epsilon}_1 \cdot \hat{\epsilon}_2^*)^2, \tag{2}$$

where ω_1 is incident energy, and the dynamic structure factor is

$$S(\mathbf{q},w) = \sum_F \left| \langle F| \sum_j \exp(i\mathbf{q}\cdot\mathbf{r}_j)|I\rangle \right|^2 \delta(E_F - E_I - \omega). \tag{3}$$

In the above equations, $r_0 = \alpha^2$ is the classical electron radius; $\hat{\epsilon}_1$ and $\hat{\epsilon}_2$ are the incoming and outgoing photon polarizations, respectively; $|I\rangle$ and $|F\rangle$ are the initial and final states with energies E_I and E_F; and $\mathbf{r}_j$ is the position operator for the jth electron. Throughout this work, we adopt atomic units where $\hbar = m = e = 1$ and $c = 1/\alpha \approx 137.036$.

For large energy transfer relative to the binding energy of a given electronic orbital of the target species, i. e. in IA, Platzman and Eisenberg have shown that the XRTS can be described approximately as a Doppler-broadened CP.[33] The energy difference is given by

$$\omega = E_f - E_i = \frac{1}{2}(\mathbf{p} + (\mathbf{k_1} - \mathbf{k_2}))^2 - \frac{\mathbf{p^2}}{\mathbf{2}} = \frac{|\mathbf{q}|^2}{\mathbf{2}} + \mathbf{q}\cdot\mathbf{p}, \tag{4}$$

where $\mathbf{p}$ is the initial momentum of the electron and $\mathbf{q}$ is the momentum transfered to it. The CP factor $J(p_q)$, defined by

$$J(p_q) \equiv \int d^3\,p\,\rho(\mathbf{p})\,\delta(p_q - (\omega/q - q/2)), \tag{5}$$

has a direct relation to the dynamic structure $S(\mathbf{q},\omega)$:

$$S(\mathbf{q},\omega) \;=\; (1/q) J(p_q). \tag{6}$$

Here, $\rho(\mathbf{p})$ is the EMD with momentum $\mathbf{p}$, and the δ function ensures energy conservation with $p_q \equiv \omega/q - q/2$. The EMD can be calculated from the real space density matrix by taking the Fourier transformation

$$\rho(\mathbf{p}) = \int d^3r\, d^3r' e^{i\mathbf{p}\cdot(\mathbf{r}-\mathbf{r}')} \rho(\mathbf{r},\mathbf{r}'). \tag{7}$$

In the RSGF approach, the real space density matrix is given by

$$\rho(\mathbf{r},\mathbf{r}') = -\frac{2}{\pi}{\rm Im}\int_{E_c}^{\infty} dE\, G(\mathbf{r},\mathbf{r}',E) f_T(E), \tag{8}$$

where $f_T(E)$ is the Fermi function. Finally, the real space Green's function $G(\mathbf{r}, \mathbf{r}', E)$ in the muffin-tin approximation is given by[34]

$$G(\mathbf{r}, \mathbf{r}', E) = -2k \left[\delta_{n,n'} \sum_L H^E_{Ln}(\mathbf{r}_>) \bar{R}^E_{Ln'}(\mathbf{r}_<) + \sum_{L,L'} R^E_{Ln}(\mathbf{r}_n)\, e^{i\delta_{Ln}} g^E_{Ln,L'n'} e^{i\delta_{L'n'}} \bar{R}^E_{L'n'}(\mathbf{r}'_{n'}) \right]. \quad (9)$$

Additional details of this formulation have been reported elsewhere.[31]

If the CP is spherically averaged over the direction of momentum transfer, the spherically averaged EMD is related by

$$\rho(p) = -\frac{1}{2\pi p} \frac{d}{dp_q} J(p_q)|_{p_q=p}, \quad (10)$$

and the following important sum rule holds for the number of the valence electrons per unit cell N:

$$N = 2\pi \int dp\, p^2\, \rho(p) = 2\pi\, \rho_0 \int dp\, p^2\, f(p). \quad (11)$$

III. DETAILS OF THE CALCULATIONS

A. MD calculations

All MD simulations reported here were performed with VASP (Viena Ab Initio Simulation Package).[35,36] Projector augmented wave (PAW) potentials[37,38] were used throughout this work, with plane wave cutoffs of 308.8 eV for Be, 140 eV for Li, and 245.7 eV for Si. For Be, the simulation cell consisted of $4 \times 4 \times 6$ repetitions of the orthogonal 4-atom conventional cell, for a total of 384 atoms. For Li, the simulation cell had 250 atoms originating from $5 \times 5 \times 5$ repetitions of the orthogonal 2-atom conventional cell. The Si simulation cell was generated from $4 \times 4 \times 4$ repetitions of the 8-atom conventional cell, for a total of 512 atoms. The temperature was controlled using the Nosé-Hoover thermostat.[39] For the range of temperatures used in this work, the thermostat s_{mass} parameter was adjusted to match the characteristic phonon frequencies, which range from 10 – 18 THz in Be,[40] 2 – 8 THz in Li,[41] and 4 – 15 THz in Si.[42]

The Be and Li MD runs used a time step of 2 fs and, for temperatures below melting, were thermalized for 8 ps. For solid Si, the time step was reduced to 1 fs and the runs were thermalized for 6 ps. For liquid Si, the system was first run at 3000 K for about 1.7 ps to ensure that the structure would be in the liquid phase. Next, the temperature was brought down to 1757 K in about 0.4 ps and thermalized for about 1.2 ps until equilibrium was reached. Given that the Fermi energies of these systems are much larger than the temperatures studied here, we set the electronic temperature to 0 K in both the MD dynamics described above and the CP calculations described in the following section.

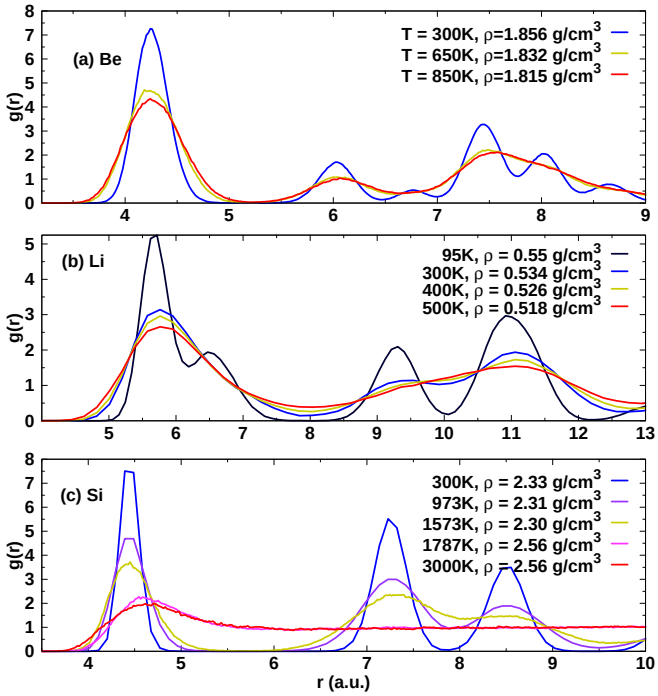

FIG. 1: Pair distribution functions $g(r)$ of Be (a), Li (b) and Si (c) as a function of temperature and adjusted densities. For Li, the density was adjusted using its linear thermal expansion coefficient ($\alpha = 46$ K^{-1}). For Si, the 3000K PDF is included to illustrate the melted behavior.

B. Compton Profile calculations

Calculations of the CP presented here were performed using the RSGF code FEFF, which does not require periodicity. FEFF includes self-consistent potentials and quasiparticle effects, and has been widely used for a variety of x-ray spectroscopies, including NIXS, which permits calculations of the core level contributions to Compton scattering. For a detailed description of the methodology used here, see Refs. 43 and 31. To get a sampling of the disordered system, we used 24 MD snapshots at temperatures above 400 K and 12 MD snapshots at temperatures below 400 K. We chose snapshots 50 to 70 fs apart in the thermalized regime. The snapshots were used to construct models for the FEFF RSGF calculations, where the cluster radii used for the calculation of the SCF potentials and FMS Green's functions were set so that the clusters would have about 170 and 260 atoms, respectively. These calculations used 13 unique self-consistent muffin-tin potentials, which roughly account for the absorber and its nearest neighbors. All other atoms outside the first coordination shell shared the same muffin-tin potential. The final CP was then calculated as an average over the CP from each structural snapshot, and the vertical bars displayed in this paper correspond to errors in the mean unless otherwise stated.

Given that the computational demand of the simulations depends greatly on the angular momentum cutoff

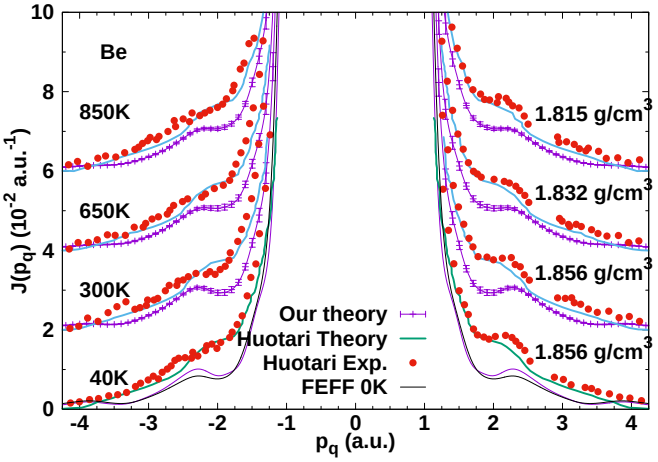

FIG. 2: Compton profiles for Be along the q = [110] direction at various temperatures and their corresponding densities.[44] Experiment and pseudopotential theory with thermal disorder[8] are included for comparison. For clarity of presentation, each data set was shifted by 0.02 electrons/a.u.. Theoretical results were broadened to match the experimental resolution of 0.16 a.u..[8]

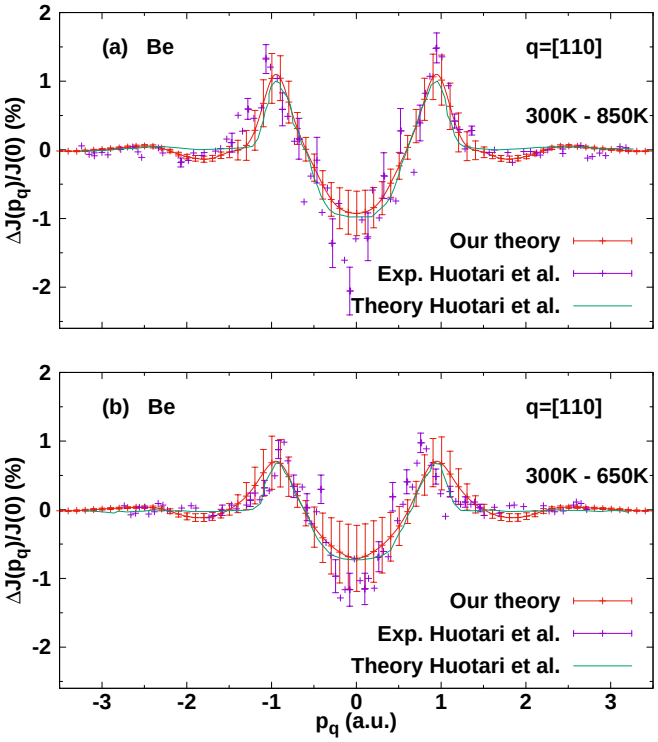

FIG. 3: Compton profile differences for Be along the q = [110] direction. Experiments and pseudopotential theory with thermal disorder[8] are included for comparison. a) 300 K - 850 K difference, and b) 300 K - 650 K difference.

$l_{\max}$, we used the lowest possible value that ensures converged results. In the cases of Li and Be, the convergence test for $l_{\max} > 3$ gives errors lower than 30% for the range of momentum values of interest. For Si, the errors are still larger for $l_{\max} \leq 4$, thus we use $l_{\max} = 5$.

Approximations made in integrating the density matrix lead to small errors (∼5%) in the number of valence electrons according to the sum rule. The CP is thus rescaled to give the proper number of valence electrons using the sum rule (Eq. 11), although the scaling is usually very close to unity. The CP is broadened by $\pi/z'_{\max}$ due to the convolution theorem, where $z'_{\max}$ is set by the FMS radius. In the cases of Be and Li, the integration bound $z'_{\max} \approx 30$ a.u., which results in a broadening on the order of 0.1 a.u..

IV. RESULTS AND DISCUSSION

One of the objectives of this study is to find signatures of temperature-driven structural change in the CP. Therefore, we begin by discussing changes in the pair distribution functions (PDFs) $g(r)$. Fig. 1 shows the PDFs for Be, Li and Si as a function of temperature. Thermal expansion was taken into account, with the system density taken from available values in the literature.[6] The Be PDF (Fig. 1a) at 300 K displays well defined peaks for the first through fifth shells. In contrast, the PDFs at 650 and 850 K show that the shells are smeared out, with the second and third shells coalescing into a single peak. Simulations of Be at ambient density and temperatures up to 2000 K show that melting occurs between 1800 K and 2000 K. Comparison with the PDF of expanded and ambient density systems shows that melting in expanded system occurs at lower temperature. Due to weaker bonding, melting in Li (Fig. 1b) occurs at lower temperatures than in Be and Si. The change in structure evidenced by the merging of the first and second shell peaks in the PDF above 95 K should affect the valence electron state probed and thus the CP. Finally, Fig. 1c shows the PDFs for Si at 1787K and 3000K. Both PDFs show the behavior of a liquid, with only the first shell peak well defined, and the two PDFs are very similar.

A. Role of disorder versus thermal expansion

1. *Beryllium*

Fig. 2 presents the CP of thermally disordered Be at finite temperature. For comparison, we also show experimental results from Huotari *et al*,[8] as well as their theoretical results[8] obtained using pseudopotential theory with disorder implemented using DWF. Coefficients for pseudopotentials were fit to match the experiment.

Although the overall intensity in our theory is underestimated, the general agreement between theory and experiment is reasonable, in particular for the position of the visible features. Contrary to what is observed for Na and Li,[13,45] Be does not show a significant sharpening of the CP as a function of thermal expansion, which is

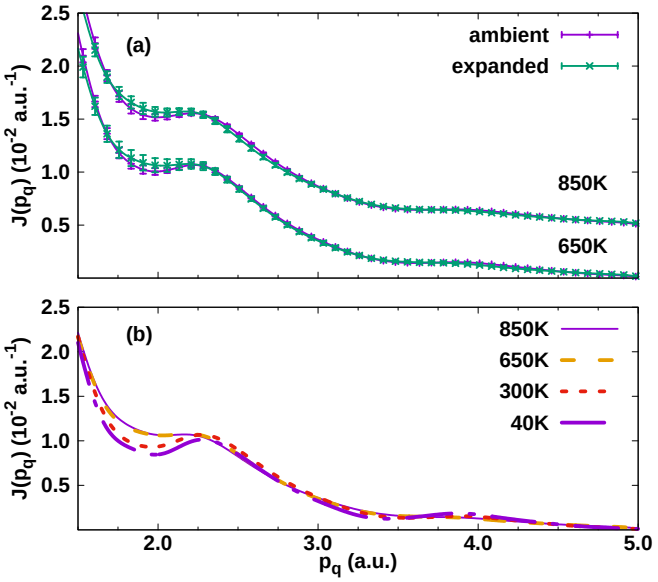

FIG. 4: CP "umklapp" peak for Be as a function of temperature. (a) Calculation of expanded and ambient density system. For clarity, results were shifted by 0.05 electrons/a.u.. (b) "Umklapp" peak region as a function of temperature.

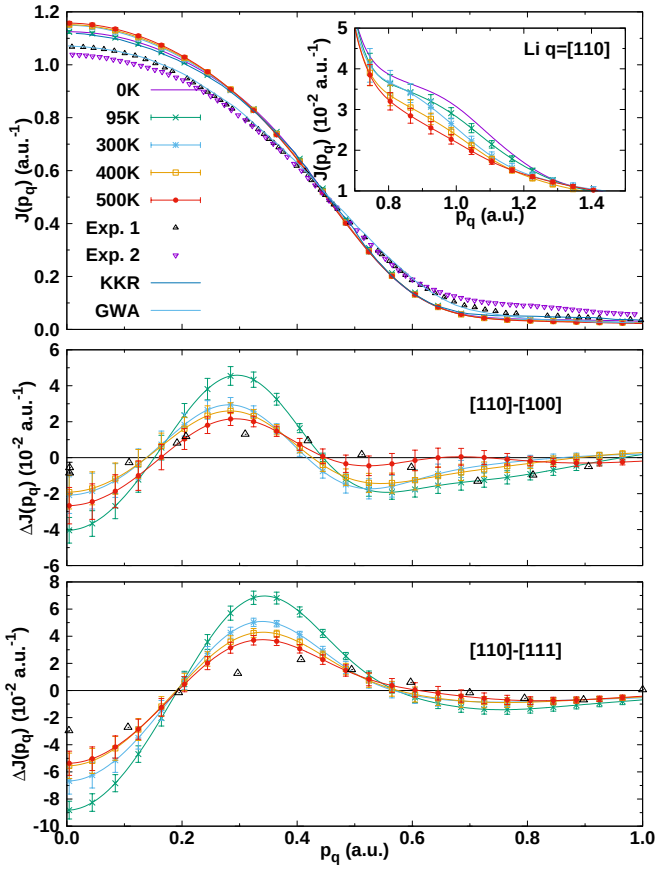

FIG. 5: Compton profiles for Li with thermal disorder as a function of temperature along the $q = [110]$ direction (top), and differences in CP between directions (center and bottom). Comparison with experimental results from Sakurai et al. ("Exp. 1")[19] and Schulke et al. ("Exp. 2")[20], and theoretical results from Schulke et al. ("KKR")[20] and Kubo et al. ("GWA")[21]. The inset in the top panel shows the "umklapp" peak amplitude in detail. The 0 K data corresponds to a calculation without disorder and at ambient density.

due to Be's smaller thermal expansion factor (α). The "umklapp" peak around $p = 2.4$ a.u. closely matches the position of the peak in the experiment.[8] This peak corresponds to a non-zero reciprocal lattice vector contribution. As the temperature is increased from 300 to 850 K, it becomes smeared out due to the thermal disorder effects. To highlight the agreement between our theory and the experiment, Fig. 3 shows the difference between the high and low temperature CPs, normalized by the CP at zero momentum.[8] As can be seen in the plot, calculated and experimental results are well within their error margins, which indicates that although our calculations underestimate the absolute value of the CP, changes are accurately reproduced. Fig. 4 shows the temperature dependence of the "umklapp peak" at 650 and 850 K as a function of thermal disorder, with and without thermal expansion. When the system is allowed to expand, the broadening is moderately enhanced due to the larger amplitude of nuclear motion, as reported by Huotari et al..[8] Temperature has only a small effect on the valence electron wave function of Be. This is likely due to its relatively high Debye temperature.

To summarize, we find that thermal expansion of Be has a moderate effect on the high component of CP. As reported in Huotari et al.,[8] thermal disorder at moderate temperature smears out the intensity of the umklapp peak. The presented calculation of Be CP is the first *ab initio* calculation with MD simulated disorder.

2. *Lithium*

Fig. 5 shows the CP for Li as a function of temperature, where the crystal structure was expanded using the experimental coefficient of thermal expansion $\alpha = 46$ K^{-1}. For comparison, experiments[19,20] and theoretical results with the KKR and GWA approximations[20,21] are also included. Our results are in good agreement with the KKR approximation with Lam-Platzman correlation corrections.[18] Both methods are based on the LDA approximation; neither takes many body effects into account. Thus, we believe that the discrepancy between the LDA and GWA results is due to many body effects. Schulke et al.[20] attributed this discrepancy to a self energy effect, due to the excitation of the plasmaron mode. The GWA results,[21] on the other hand, are in very good agreement with the experiment. The same authors have performed LDA calculations with correlation effects,[46]

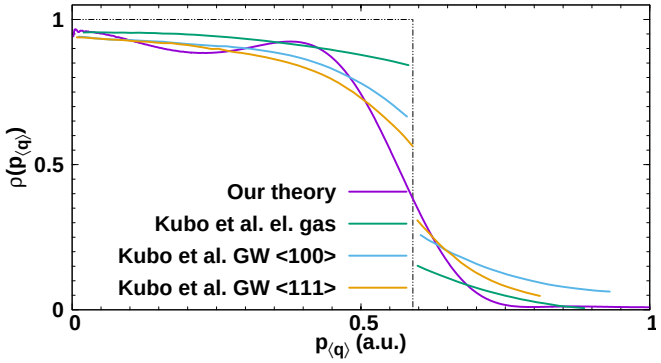

FIG. 6: Valence EMD for Li calculated using RSGF, Fermi gas model and GW approximation.[21]

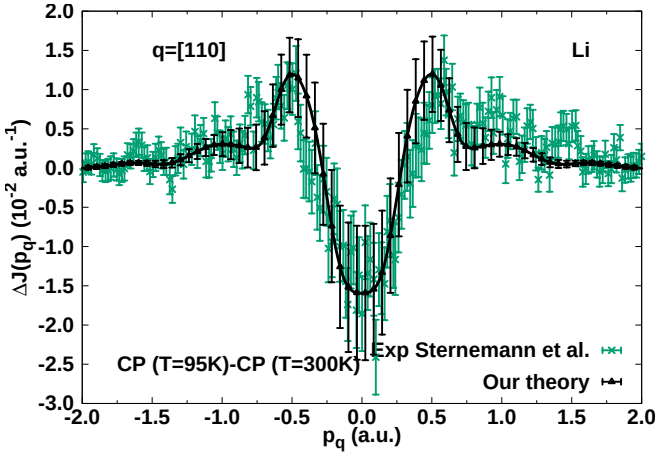

FIG. 7: Differences in calculated CP of Li for q = [110] between T = 95 K and T = 300 K and comparison with experiment.[9]

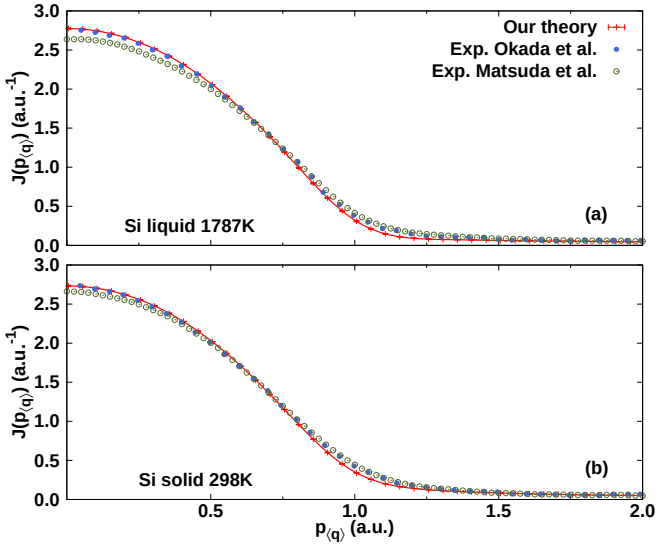

FIG. 8: Comparison of the calculated and experimental results for[6,47] the CP of Si in liquid phase (a) and polycrystalline solid phase (b).

which reduce the discrepancy between LDA and the experiment. The GWA method provides better results than the corrected LDA, but it was emphasized[22] that GWA calculations by Kubo have an unphysical behavior of the imaginary part of the self-energy at the Fermi level. The EMD $\rho(\mathbf{p}) = \sum_b \pi^{-1} \int_{-\infty}^{\mu} \mathrm{Im}\, G_{b,b}(\mathbf{p}, E) dE$ in the LDA approach was obtained using the Fermi gas model and is different from the EMD obtained in the GW approximation. Our results for the EMD of Li are shown in Fig. 6 for the system at 0 K, and compared to both the Fermi gas model and the GW approximation.[21] The differences between the theories in Fig. 6 highlight how much the many-body effects influence the EMD.

In contrast to previously reported LMTO calculations of Li,[13,45] we do not observe broadening of the CP as thermal disorder increases. The inset in Fig. 5 shows the behavior of the "umklapp" peak as a function of both thermal expansion and thermal disorder. Although it behaves similarly to Be, in the case of Li the peak essentially disappears above 400 K, likely due to the fact that Li is a softer material with a much lower Debye temperature.

In order to study the anisotropy of the CP, the lower panels of Fig. 5 present differences between directional CPs, labeled accordingly, together with experimental results.[20] We find that the oscillation amplitudes decrease as a function of temperature, with the largest amplitude observed at 95 K. The largest anisotropy occurs in the [110] − [111] directions difference. Although our results follow the oscillation pattern in the experiment, discrepancies due to neglecting many-body effects are still noticeable. Our calculations generally become closer to the experiment with increasing temperature.

The differences between the CPs calculated at 95 K and 300 K are presented in Fig. 7 and compared to experimental measurements of thermally disordered Li along the $q = [110]$ direction of momentum transfer.[9] With the exception of a small discrepancy in the position of the peak at around 0.5 a.u., which is likely due to the use of a constant value for the thermal expansion coefficient, our results are in good agreement with the experiment.

3. *Silicon*

Finally, we study the CPs of solid and liquid Si. Our results (Fig. 8) are in fair agreement with recent experiments[6,47] for a broad range of momentum p_q.

To study the effects of melting, Fig. 9 shows differences between the CPs of solid Si at 298 K and liquid Si at 1787 K. Our results are shown for angular momentum cutoffs $l = 5$, together with experimental and theoretical results.[6,47] Our calculations agree reasonably well with experimental results, in particular those from Okada et al.[6] The differences between our theory and the CPMD results arise both from the differences in the methodologies used to compute the CP, i.e. our RSGF approach *vs* momentum based theory, and from differences in MD

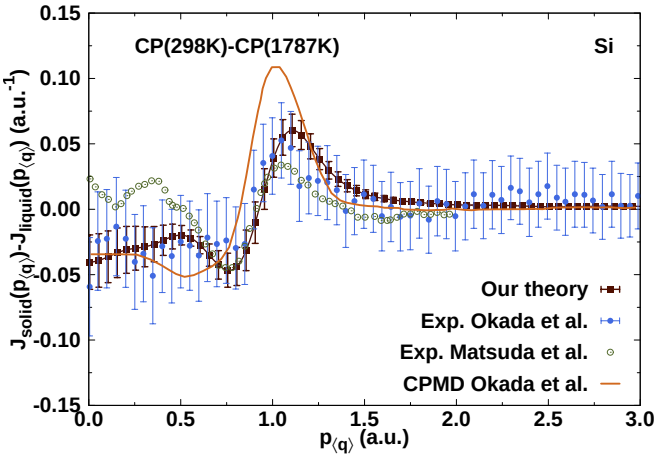

FIG. 9: Differences in polycrystalline Si CP calculations for angular momentum $l = 5$ between T = 300 K (solid) and T = 1757 K (liquid) and CPMD calculations, in comparison with experiments.[6,47]

simulations.

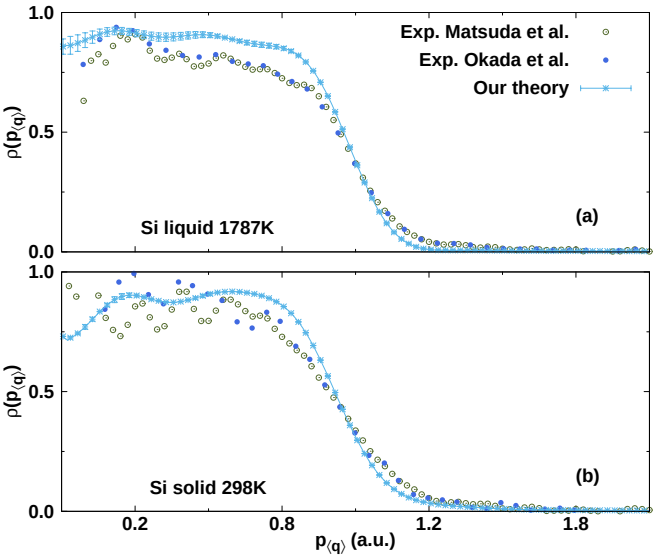

FIG. 10: (a) Valence EMD for Si at T = 298K and comparison with experiments.[6,47] (b) Valence EMD for Si at T = 1787K and comparison with experiments.[6,47]

Figure 10 presents the EMD for solid and liquid Si at 298 and 1787 K, respectively, and comparison with experimental values obtained from the experimental CPs.[6,47] Although we achieved good agreement between our theory and the experimental results for both CP and for changes in the CP in solid-liquid transitions, some noticeable differences remain between EMDs in out theory and those in the experiment. The differences in the EMD results might be due to the many body effects, which do not strongly affect CP.

V. CONCLUSIONS

In summary, we have presented RSGF calculations of the CP coupled with MD simulations to model thermal disorder for Be, Li and Si for a number of temperatures. We find that our calculations are in good agreement with experiments and other theories. We investigated both thermal disorder and thermal expansion effects on the high momentum components of the CP. We find that the lattice thermal expansion has a moderate effect on the CP in both Be and Li, as previously reported. Thermal disorder has the effect of smearing the high momentum "umklapp" peak of Be and Li. Our results also predict changes in the CP of polycrystalline Si, which undergoes a solid to liquid phase transition, to a good degree of precision. We observe that in the case of Li, strong directional anisotropy, which was discussed in the recent work on LiF[25] as a function of thermal disorder, becomes weaker as a function of temperature.

For temperatures close to the melting point, both thermal disorder and thermal expansion play an important role and need to be taken into account when studying the electronic properties of Be and Li. For Si structure, which undergoes a solid – liquid phase transition, disorder has an important role and MD simulations coupled with real space theory can reasonably predict the influence of the disorder on the CP.

We have shown that the RSGF approach combined with DFT-MD is a reliable method for predicting the CP of disordered systems. In addition, the RSGF approach is not limited to crystalline systems and permits efficient calculations of valence electron properties of the materials as a function of thermal disorder and thermal expansion. Electronic temperature effects are also naturally included in the approach. It is thus ideally suited for studies of highly disordered materials across a wide range of temperatures, from zero to the WDM regime, where solid state effects are still not well understood. A more detailed application to the WDM regime, including ionic as well as electronic temperature effects, remains as straightforward procedure for future studies.

VI. ACKNOWLEDGMENTS

This work is supported by in part by DOE BES Grant No. DE-FG03-97ER45623. This work was also supported by the Office of Science, Fusion Energy Sciences and the National Nuclear Security Administration thought Grant No. DE-SC0008580. We also thank Professor Kazuhiro Matsuda and Dr. Nozomu Hiraoka for providing CP Si experimental results. This research used resources of the National Energy Research Scientific Computing Center (NERSC), a DOE Office of Science User Facility supported by the Office of Science of the U.S. Department of Energy.

[1] M. Cooper, P. Mijnarends, N. Shiotani, N. Sakai, and A. Bansil, *X-ray Compton scattering* (OUP Oxford, 2004).
[2] Y. Sakurai, M. Itou, B. Barbiellini, P. Mijnarends, R. Markiewicz, S. Kaprzyk, J.-M. Gillet, S. Wakimoto, M. Fujita, S. Basak, et al., Science **332**, 698 (2011).
[3] B. Barbiellini, C. Bellin, G. Loupias, T. Buslaps, and A. Shukla, Phys. Rev. B **79**, 155115 (2009).
[4] M. Hakala, K. Nygård, S. Manninen, S. Huotari, T. Buslaps, A. Nilsson, L. Pettersson, and K. Hämäläinen, J. Chem. Phys. **125**, 084504 (2006).
[5] M. Hakala, K. Nygård, J. Vaara, M. Itou, Y. Sakurai, and K. Hämäläinen, J. Chem. Phys. **130**, 034506 (2009).
[6] J. T. Okada, P. H.-L. Sit, Y. Watanabe, Y. J. Wang, B. Barbiellini, T. Ishikawa, M. Itou, Y. Sakurai, A. Bansil, R. Ishikawa, et al., Phys. Rev. Lett. **108**, 067402 (2012).
[7] J. T. Okada, P. H.-L. Sit, Y. Watanabe, B. Barbiellini, T. Ishikawa, Y. J. Wang, M. Itou, Y. Sakurai, A. Bansil, R. Ishikawa, et al., Phys. Rev. Lett. **114**, 177401 (2015).
[8] S. Huotari, K. Hämäläinen, S. Manninen, C. Sternemann, A. Kaprolat, W. Schülke, and T. Buslaps, Phys. Rev. B **66**, 085104 (2002).
[9] C. Sternemann, G. Doring, C. Wittkop, W. Schulke, A. Shukla, T. Buslaps, and P. Suortti, J. Phys. Chem. Solids **61**, 379 (2000).
[10] O. K. Andersen, Phys. Rev. B **12**, 3060 (1975).
[11] T. Jarlborg and G. Arbman, J Phys F Met Phys **7**, 1635 (1977).
[12] T. Jarlborg and P. Lerch, Phys. Lett. A **176**, 130 (1993).
[13] S. Dugdale and T. Jarlborg, Solid State Commun. **105**, 283 (1998).
[14] K. Chen, V. Caspar, C. Bellin, and G. Loupias, Solid State Commun. **110**, 357 (1999).
[15] C. Sternemann, T. Buslaps, A. Shukla, P. Suortti, G. Döring, and W. Schülke, Phys. Rev. B **63**, 094301 (2001).
[16] J. Korringa, Physica **13**, 392 (1947).
[17] A. Bansil, R. S. Rao, P. E. Mijnarends, and L. Schwartz, Phys. Rev. B **23**, 3608 (1981).
[18] L. Lam and P. M. Platzman, Phys. Rev. B **9** (1974).
[19] Y. Sakurai, Y. Tanaka, A. Bansil, S. Kaprzyk, A. T. Stewart, Y. Nagashima, T. Hyodo, S. Nanao, H. Kawata, and N. Shiotani, Phys. Rev. Lett. **74**, 2252 (1995).
[20] W. Schülke, G. Stutz, F. Wohlert, and A. Kaprolat, Phys. Rev. B **54**, 14381 (1996).
[21] Y. Kubo, J. Phys. Soc. of Jpn. **66**, 2236 (1997).
[22] W. Schülke, J. Phys. Soc. of Jpn. **68**, 2470 (1999).
[23] H. Bross, Phys. Rev. B **72**, 115109 (2005).
[24] T. Baruah, R. R. Zope, and A. Kshirsagar, Phys. Rev. B **60**, 10770 (1999).
[25] A. Erba, J. Maul, M. Itou, R. Dovesi, and Y. Sakurai, Phys. Rev. Lett. **115**, 117402 (2015).
[26] J. P. Perdew, A. Ruzsinszky, G. I. Csonka, O. A. Vydrov, G. E. Scuseria, L. A. Constantin, X. Zhou, and K. Burke, Phys. Rev. Lett. **100**, 136406 (2008).
[27] A. Romero, P. Silvestrelli, and M. Parrinello, Phys. Status Solidi B **220**, 703 (2000).
[28] A. H. Romero, P. L. Silvestrelli, and M. Parrinello, J. Chem. Phys. **115**, 115 (2001).
[29] R. Car and M. Parrinello, Phys. Rev. Lett. **55**, 2471 (1985).
[30] J. A. Soininen, A. L. Ankudinov, and J. J. Rehr, Phys. Rev. B **72**, 045136 (2005).
[31] B. A. Mattern, G. T. Seidler, J. J. Kas, J. I. Pacold, and J. J. Rehr, Phys. Rev. B **85**, 115135 (2012).
[32] W. Schülke, *Electron dynamics by inelastic X-ray scattering* (OUP Oxford, 2007).
[33] P. Eisenberger and P. M. Platzman, Phys. Rev. A **2**, 415 (1970).
[34] M. P. Prange, J. J. Rehr, G. Rivas, J. J. Kas, and J. W. Lawson, Phys. Rev. B **80**, 155110 (2009).
[35] G. Kresse and J. Hafner, Phys. Rev. B **47**, 558 (1993).
[36] G. Kresse and J. Hafner, Phys. Rev. B **49**, 14251 (1994).
[37] P. E. Blöchl, Phys. Rev. B **50**, 17953 (1994).
[38] G. Kresse and D. Joubert, Phys. Rev. B **59**, 1758 (1999).
[39] S. Nose, J. Chem. Phys. **81**, 511 (1984), ISSN 0021-9606.
[40] R. Stedman, Z. Amilius, R. Pauli, and O. Sundin, J. Phys. F: Met. Phys. **6**, 157 (1976).
[41] D. C. Wallace, Phys. Rev. **178**, 900 (1969).
[42] G. Dolling, in *Inelastic Scattering of Neutrons in Solids and Liquids. V. II. Proceedings of the Symposium on Inelastic Scattering of Neutrons in Solids and Liquids* (1963).
[43] J. J. Rehr, J. J. Kas, M. P. Prange, A. P. Sorini, Y. Takimoto, and F. D. Vila, C. R. Phys. **10**, 548 (2009).
[44] J. R. Jeffries, private communication.
[45] C. Filippi and D. M. Ceperley, Phys. Rev. B **59**, 7907 (1999).
[46] B.I. Lundqvist, Phys. Konden. Mater. **7** (1968).
[47] K. Matsuda, T. Nagao, Y. Kajihara, M. Inui, K. Tamura, J. Nakamura, K. Kimura, M. Yao, M. Itou, Y. Sakurai, et al., Phys. Rev. B **88**, 115125 (2013).